Tellus (2000), 52B, 1189–1205
Printed in UK. All rights reserved

TELLUS
ISSN 0280–6509

Numerical modeling of pollutant transport and chemistry during a high-ozone event in northern Taiwan

By ZIFA WANG[1], WEIMING SHA[2] and HIROMASA UEDA[3]*, [1]*Disaster Prevention Research Institute, Kyoto University, Uji, Kyoto 611-0011, Japan; and State Key Laboratory of Atmospheric Boundary Physics and Atmospheric Chemistry, Institute of Atmospheric Physics, Chinese Academy of Sciences, Beijing, 100029, China;* [2]*Geophysical Institute, Graduate Scholl of Science, Tohoku University, Aoba-ku, Sendai, Miyagi 980-8578, Japan;* [3]*Disaster Prevention Research Institute, Kyoto University, Uji, Kyoto 611-0011, Japan*

(Manuscript received 25 February 1999; in final form 16 February 2000)

ABSTRACT

An air pollution prediction model system (APOPS) is developed and applied to northern Taiwan with complex terrain and local thermal circulations. It consists of a nonhydrostatic mesoscale meteoro-logical model system (MMPMS) and a gas/aerosol transport and air quality model (GATAM). The basic processes relevant to modeling the urban air pollution problems such as meteorology, dispersion, chemistry and deposition are solved at the same time on practically the same grid. The APOPS was tested on a high-ozone event in northern Taiwan on 16 November 1998. Comparison with observed surface winds shows able to predict local flow patterns such as sea/land breezes and mountain-valley wind in this high air pollution episode. The predicted surface concentrations of ozone and other pollutants are compared with measured values, and a fairly good agreement with the mean normalized biases of −6%, −11%, for one-day simulation and for daytime, respectively, is obtained for ozone. Thus, it is confirmed that the APOPS can be utilized to predict urban air quality in complex terrain area.

1. Introduction

Taiwan's location off the south coast of China puts it under the influence of Asian monsoon system. It is also located between the Asian continent, the South China Sea and North Pacific Ocean and is therefore in a zone where different types of air mass meet. The economy and industry of Taiwan have been developed rapidly in the past 30 years, with abundant trace gases emitted from anthropogenic sources. Based upon the monitoring records of recent years, air quality in Taiwan continues to show improvement, the annual ratio of days with PSI greater than 100 being less than 6% in 1997. However, the averaged ozone concentration increased by 8.1% from 1994 to 1996. Thus, Taiwan is still experiencing one of the worst air qualities on the globe and requiring continued efforts to meet the air quality standard. Taipei, a well-known densely populated mega-city with heavy traffic, is the rapidly expanding capital city of Taiwan, located in a basin surrounded by mountains on 3 sides and by 2 river valleys reaching northwesterly and northeasterly to the Pacific Ocean (Fig. 1). A high level of ozone has been a serious problem in Taipei (Liu et al., 1990). The local-scale circulations and airflow would be very complex in this region due to the very complex terrain and the special location. The combination of special meteorological conditions and high emissions in the area may result in very

* Corresponding author.
e-mail: ueda@storm.dpri.kyoto-u.ac.jp

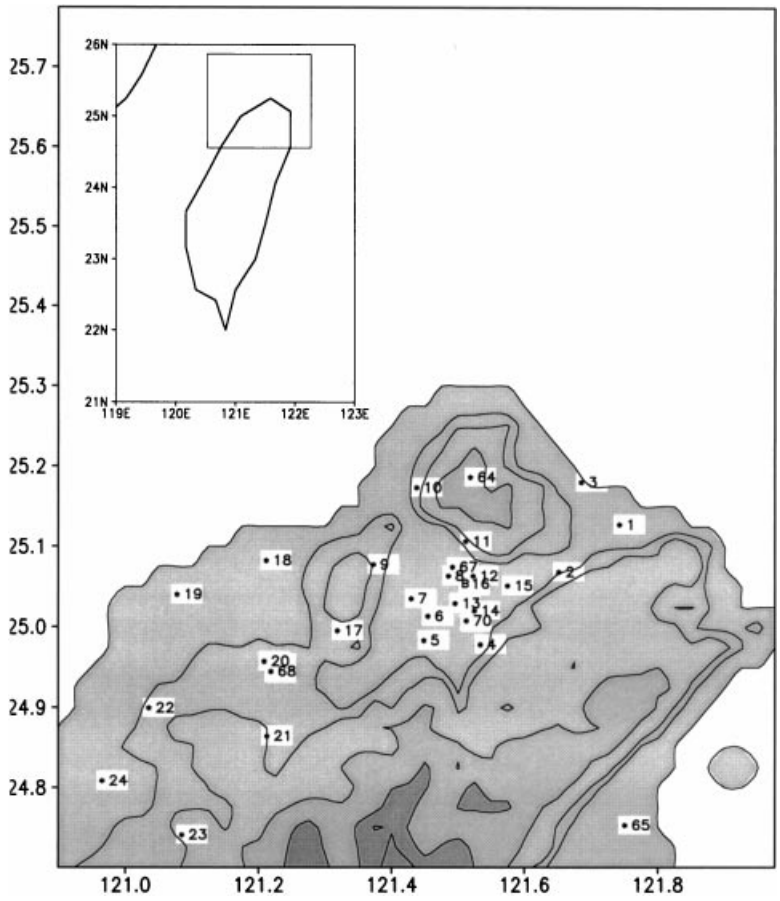

Fig. 1. Model domain and topography. Dots representing air monitoring stations are indicated. Solid lines are the height contours of 0, 200, 500, 1000 m MSL.

high concentrations of photochemically-produced pollutants.

Numerical models are a relatively inexpensive and expedient means of gaining insight into the meteorological and chemical processes that give rise to the high concentration of pollutants. Many air quality models have been developed (Yamartino et al., 1992, 1993; Scheffe and Morris, 1993; Moussiopoulos, 1995; Svensson, 1995a). Some are applied extensively to simulate the surface concentrations of pollutants using the wind fields derived by the objective analysis of wind observations. However, such diagnostic winds can be limited in accuracy by the temporal and spatial resolutions of the networks. The limitation in accuracy is severe, in particular when local thermal circulations are prevailing over complex terrain, since at that time, heavy air pollution is often caused. Thus, a few air quality models (Chang et al., 1987; Svensson, 1995a; Lu and Turco, 1997) use the wind fields predicted by meteorological models. A few applications of such models have been carried out in cities in Japan, Europe, the US and Australia (Kitada and Kitagawa, 1990; Wakamatsu et al., 1998; Svensson, 1995b; Buckley and Kurzeja, 1997a, 1997b; Hurley and Manins, 1995).

However, this has not been done for Taiwan. When simulating air-quality in such a region with complex terrain and local thermal circulation, it is crucial to solve the meteorology and chemistry at the same time on practically the same grid as

possible. In this paper, an air pollution prediction model system (APOPS) is described and applied to predict a high ozone episode on 16 November 1998. Section 2 includes analysis of the photochemical characteristics by means of air monitoring data from the TAQMN (Taiwan Air Quality Monitoring Network) under the synoptic meteorological conditions leading to the high ozone event. The APOPS is briefly described in Section 3. Details of simulations conducted for the high-ozone episode and assessment of predicted surface winds, ozone and other pollutants with observation data are provided in Section 4. Major conclusions are summarized in Section 5.

2. Data analysis for the high-ozone episode

Hourly mean ground level concentrations of sulfur dioxides (SO_2), nitrogen oxides (NO_X), carbon monoxide (CO), ozone (O_3), aerosols (PM10) from the TAQMN are used for analysis. The TAQMN has totally 71 air monitoring stations distributed in Taiwan. Among these stations, 29 are located in our model domain, including 23 ambient air-quality monitoring stations, 3 traffic area stations, 2 background stations and 1 national park station (Fig. 1). An episode during 15–17 November was selected for a case study as the 1-h averaged ozone concentrations over the 100 ppb level were recorded at many locations.

The surface-level synoptic pattern associated with such a high-ozone episode is characterized by a high-pressure system. A small high-pressure system over the southeast China was slowly moving to Taiwan on 15 November. On 16 November, a strong Mongolian high-pressure system moved eastward and covered the whole continent of eastern Asia, while a low-pressure system was situated over the Japan Sea. Thus, the gradient wind over northern Taiwan was very weak and local sea/land breezes were predominant under this relatively stationary synoptic situation. On 17 November, Taiwan was controlled by the winter monsoon with the prevailing northeasterly winds again.

The high concentration of ozone and other pollutants were observed in northern Taiwan on 16 November under the weak gradient wind situation. Fig. 2 shows the observed concentrations of ozone and other pollutants averaged for 11 stations within the Taipei basin. A time series of observed wind and pollutant concentration distributions are presented in Fig. 3 for 24 stations in the model domain from 15–17 November. The wind speed was very low on 16 November, especially for the stations in the Taipei basin, i.e., locations 4–13 (Fig. 3a). The diurnal variation of wind direction was complex, but exhibited the characteristics of the sea/land breeze. The wind speed increased much more after 8:00 LT on 17 November due to the influence of the strong northeasterly winter monsoon.

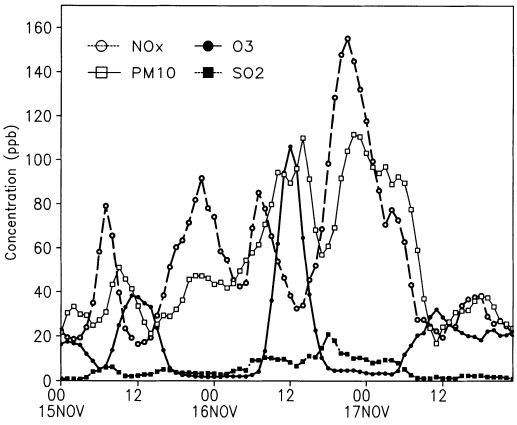

Fig. 2. Time series plots of observed NO_X (ppb), O_3 (ppb), SO_2 (ppb) and PM10 ($\mu g/m^3$) concentrations averaged for 11 stations located within the Taipei basin.

The highest O_3 concentration was observed in the Taipei basin with a peak value of 118 ppb near noon-time on 16 November (Fig. 2). High values of ozone concentration, with a peak more than 100 ppb around noon-time were also observed at many stations (Fig. 3). The well-recognized single peak (SP) pattern suggested the dominant rôle of the in situ photochemical formation due to the maximum of temperature and solar radiation at midday.

Although the O_3 levels on the other days were lower, i.e., less than 40 ppb. it was noted that after 18:00 LT and before the next 6:00 LT, the mean ozone levels remained at consistently low values in the center of Taipei. The low levels of ozone at night probably resulted from the depletion by the reaction with high-level NO_X. It was in great contrast with the ozone concentrations at 2 background stations 3 and 19 (Fig. 3) at which they had not decreased to a very low level at night.

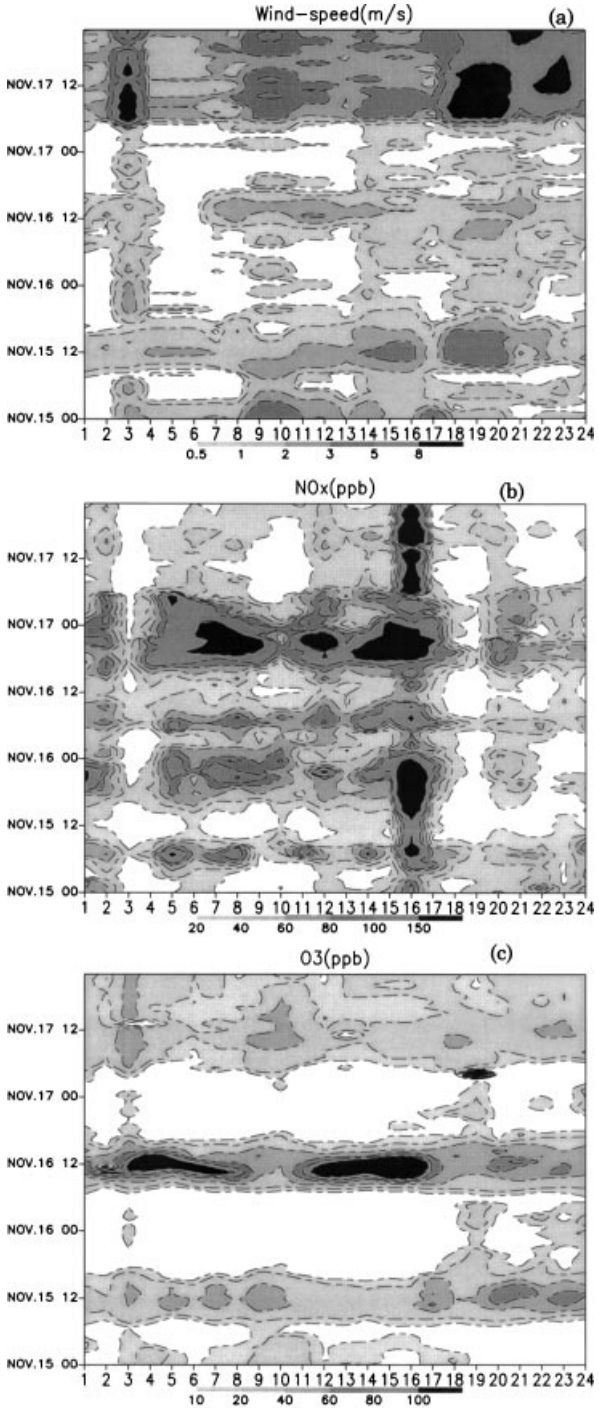

Fig. 3. Observed time series of (a) wind speed (m/s), (b) NO_X (ppb), and (c) O_3 (ppb) from 15–17 November 1998 at 24 stations in northern Taiwan. The numbers below the horizontal axis represent the locations shown in Fig. 1.

Nitrogen oxides, along with volatile organic components (VOCs), are primary ozone precursors. All the stations exhibited a similar diurnal pattern of NO_X which consisted of 2 peaks in the early morning around 9:00 LT and in the evening around 21:00 LT, except for 2 background stations 3 and 19 (Fig. 3). Troughs of the concentration pattern between the 2 peaks at midday were mainly caused by the thicker mixing layer, lower emission and photochemical consumption. The concentration of NO_X on 17 November was relatively low because of the strong northeasterly winds. The highest level of NO_X was observed for all time at stations 15–17, which represent the center of Taipei. The level of SO_2 was rather low in Taipei with a small peak in the afternoon of 16 November, but particle matters PM10 had very high concentration with double peaks of 105 $\mu g\ m^{-3}$.

3. Description of the air pollution prediction model system (APOPS)

Eulerian grid models are the most complex, but potentially the most powerful, air quality models, involving the least restrictive assumptions. With a finite difference approximation, the grid models solve a set of transport and diffusion equations including the temporal and spatial variation of the meteorological variables, pollutant emissions and surface characteristics. The structure of APOPS is shown in Fig. 4. The elements of the system are interconnected to provide a more comprehensive treatment of the complex interactions between chemistry and dynamics in the regional setting. The system requires spatially and temporally resolved emissions, topographic features, initial meteorological conditions and background pollutant concentrations. Meteorological variables to drive the advection, turbulent diffusion, deposition and chemical processes of pollutants are supplied by the meteorological model, i.e., MMPMS.

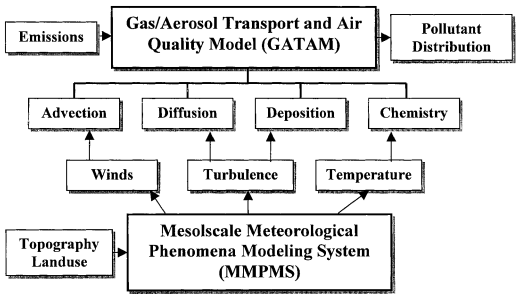

Fig. 4. Structure of the air pollution prediction model system (APOPS).

The model equations for meteorology and chemical transport are solved on practically the same grid in a terrain-following coordinate (η) system with

$$\eta = \frac{z-h}{H-h}, \tag{1}$$

where $h(x, y)$ is the height of the topography and H is the top height of the model.

3.1. *MMPMS: the meteorological model*

A 3-dimensional, non-hydrostatic, terrain-following numerical model (MMPMS) is used to investigate the dynamics of meteorological fields with an appropriate turbulence scheme. The model has been extensively and successfully applied to study the dynamics of the sea/land breezes and Adelaide gully wind of South Australia and combinations of thermal circulations in the Kanto Plain in Japan (Sha et al., 1991, 1993, 1996). Thus, it has been shown to give good predictions of meteorological fields in the regions with complex terrain and prevailing local thermal circulations both in 2- and 3-dimensional simulations.

The governing equations are based on the atmospheric primitive equations simplified by the anelastic and Boussinesq approximations. The vertical eddy diffusivity for momentum K_V is determined from the turbulent kinetic energy E and its dissipation rate ε, and the horizontal eddy diffusivity K_H is given by a nonlinear three-dimensional form. The surface temperature T_g is determined by solving the energy budget equation at the earth's surface (Sha et al., 1996).

The prognostic equations presented in the section are integrated forward explicitly in time with the time step selected by the Courant–Friedrichs–Leury (CFL) criterion. A centered difference approximation is used in space; the advection terms are evaluated by an upstream difference with a spline technique. The mesoscale pressure, p', is computed by solving a 3-dimensional discrete Poisson equation with a Neumann boundary

condition. The equation is solved directly by Gaussian elimination in the vertical and by function decomposition with fast Fourier transforms in the horizontal directions.

3.2. *GATAM: the tracer chemical transport model*

In essence, the time rate of change of a pollutant depends on advection, diffusion, emission, deposition and chemical reaction of the pollutant. The gas/aerosol transport and air quality model (GATAM) are designed to compute the concentration of atmospheric trace species based on the numerical solution of a set of n coupled, nonlinear diffusion equations. The dynamics of each species i are mathematically described by the terrain following system (η) of the conservation equations:

$$\frac{\partial C_i}{\partial t}+\frac{\partial(u\cdot C_i)}{\partial x}+\frac{\partial(v\cdot C_i)}{\partial y}+\frac{1}{H-h}\frac{\partial(w\cdot C_i)}{\partial \eta}$$
$$=\frac{\partial}{\partial x}\left(K_{\mathrm{H}}\frac{\partial C_i}{\partial x}\right)+\frac{\partial}{\partial y}\left(K_{\mathrm{H}}\frac{\partial C_i}{\partial y}\right)$$
$$+\frac{1}{H-h}\frac{\partial}{\partial \eta}\left(K_{\mathrm{V}}\frac{\partial C_i}{\partial \eta}\right)+S_i+R_i+D_i, \qquad (2)$$

where C_i is the concentration of species i, R_i is the net production (depletion if negative) of species i by chemical reaction, S_i is the emission rate and D_i is the deposition term. The cloud and precipitation processes are not considered in the simulation of this paper. Here, u, v, w are the components of wind velocity, K_{H} and K_{V} are the horizontal and vertical diffusion coefficients. Distributions of these parameters, as well as temperature are crucial to simulate the air quality in regions with complex terrain and local thermal circulation and to estimate reaction rate coefficients. In the present prediction model system, they are predicted by MMPMS.

A simplified but very accurate mass conservative, peak-preserving, mixing ratio bounded advection algorithm is used to solve the 3-dimensional mass conservation eq. (2) by a time-splitting technique (Carmichael et al., 1986; Walcek and Aleksic, 1998).

The solution of the above equation requires specification of initial and boundary conditions. The initial surface mixing ratios of NO, NO_2, CO, SO_2, O_3 and aerosols (PM10) are horizontally interpolated from the available observed data of the TAQMN at the beginning of the simulation. Above this height, the mixing ratios of these species are assumed to decrease exponentially with the characteristic length scale for each species (Chang et al., 1989). Here, the top boundary concentration of ozone is assigned to be 30 ppb, while those for other species are zero. The boundary conditions used to solve eq. (2) are set as follows: pollutants except for ozone can only be allowed to transport out of and not into the side-boundaries. For ozone, the background concentration profile is assumed to be 20 ppb at the surface and change exponentially to 30 ppb at the top boundary. The concentration at the top boundary is assumed to remain constant during the simulation. The ground-level boundary condition is a statement of the balance between deposition, vertical diffusion and ground-level emission:

$$S_i-v_{\mathrm{d}}\cdot C_i=-K_{\mathrm{V}}\frac{1}{H-h}\frac{\partial C_i}{\partial \eta}. \qquad (3)$$

The dry deposition parameterization is based on Chang et al. (1987) and Wang et al.(1996).

Emission of chemical components is crucial to the resulting concentration of the model simulation. The emission inventory used here is interpolated from the original data provided by the Environmental Protection Administration (EPA) of Taiwan. No biogenic emission is included. The major sources of air pollution in Taiwan can be divided into 2 categories: stationary sources, represented by 90,000 factories, and mobile sources, referring to 13 million currently operating vehicles in 1996. In 1996, the total emission of particulate matter (PM10) reached 636,200 metric tons, caused by civil constructions, industrial processing, and fuel burning. 748,000 metric tons of the nitrogen oxides and 532,000 metric tons of sulfur oxides were emitted principally from generating electricity, diesel fuel vehicles and industrial processing. Total emissions for non-methane hydrocarbon were 1,089,700 metric tons on account of oil refinery industries, industrial solvent usage, and operating vehicles. Table 1 gives the

Table 1. *List of the emission amounts (10^3kg/day) valid for the model domain*

Species	PM10	SOX	NOX	NMHC
Total	753	243	727	1608

total daily emissions of some species in our model domain. The height of emissions is set at the lowest level of the model. The diurnal variation of emissions from traffic is taken into account in the model, but that from industries is ignored in the present stage of the simulation. It is because the contribution from the industrial emissions is suspected not to be dominant on the air quality in the Metropolitan area and its surroundings, as seen from the very low SO_x concentration and high NO_x, and because the inventory of the diurnal variation in the industrial emission is not available. Obviously, the emission inventory used in the present investigation, which is suspected to have about 20% error (Liu et al., 1999), is just an approximation to the actual sources of primary pollutants in the northern Taiwan region. Thus, a sensitivity test of emission reduction is made and compared with the base case in Subsection 4.4.

3.3. Reaction mechanism scheme

To present an accurate description of the atmospheric transformation rates, a transport model must include a gas-phase chemical mechanism that incorporates all significant chemical reactions. However, such a presentation of the gas-phase transformation has to be simplified for the very complex chemistry in the real atmosphere, since it is still impossible for current computer resources to run a complex transport model together with the very complex chemical transformation model. Comparing with a number of gas-phase chemistry mechanisms used in studies of Los Angles smog, Dodge (1989) showed that the Carbon-Bond IV (CBM-IV) (Gery et al., 1989) and SAPRC (Carter et al., 1986) mechanisms are reasonably in agreement with a common database of environmental chamber experiments at room temperature. The gas-phase chemical reaction scheme used in the present work is a slightly modified version of the CBM-IV (Gery et al., 1989; He and Huang, 1992). Values of the reaction rate coefficient are updated with recent kinetic data, and more detailed chemistry of SO_x is incorporated (Wang et al., 1996). The modified mechanism includes 34 species and 86 photochemical, inorganic and organic reactions. It is executed by the chemistry model and the result is subjected to the transport model calculations. 11 active species are predicted from the full equation of mass conservation including advection and diffusion, while reactive agents like radicals are calculated from the pseudo equilibrium assumption. The scheme is addressed especially for the accurate modeling of ozone which is produced photochemically from the mixture of nitrogen oxides and hydrocarbons, and it is therefore the best suited for use when ozone is the pollutant in focus.

3.4. Simulation setup

The model domain and the topography of Taiwan are shown in Fig. 1. The domain is divided into 71×51 regular grids in the horizontal direction with 3-km resolution, covering northern Taiwan from 120.83°E to 122.4°E and 24.63°N to 25.8°N. Vertically, the model uses 40-layer terrain following the coordinate system, with the model top being 7400 m above sea level. Vertical-grid spacing is increased gradually from 10 m at the surface to 300 m at the top. This grid system is used both in the meteorological and chemical transport models. The height of the topography is obtained from the global elevation datasets (GTOPO30) developed by the US Geographical Survey's EROS Data Center with a horizontal resolution of 30 arc s.

The 24-h simulation is initiated at 0:00(LT) on 16 November 1998 with interpolated reanalysis data from the ftp service (http://ftp.ncep.noaa.gov) of the National Centers for Environmental Prediction (NCEP), as the initial condition for MMPM. The data set includes information about pressure, temperature, dew point, wind speed, and wind direction at numerous altitudes. The sea-surface temperature is kept at a constant value (296 K) for the whole run. The soil temperature as the initial condition is assumed to be uniform at 0:00 LT and equal to the surface air-temperature given by the NCEP dataset.

4. Results and model evaluation

4.1. Wind fields

Fig. 5 shows the simulated wind field at $z =$ 10 m above ground for 06:00, 10:00, 12:00, 14:00, 16:00, and 20:00 LT, respectively. Thick arrows represent observed surface wind vectors. The observed winds in the coastal area obviously show the diurnal variation of the sea/land breezes. In

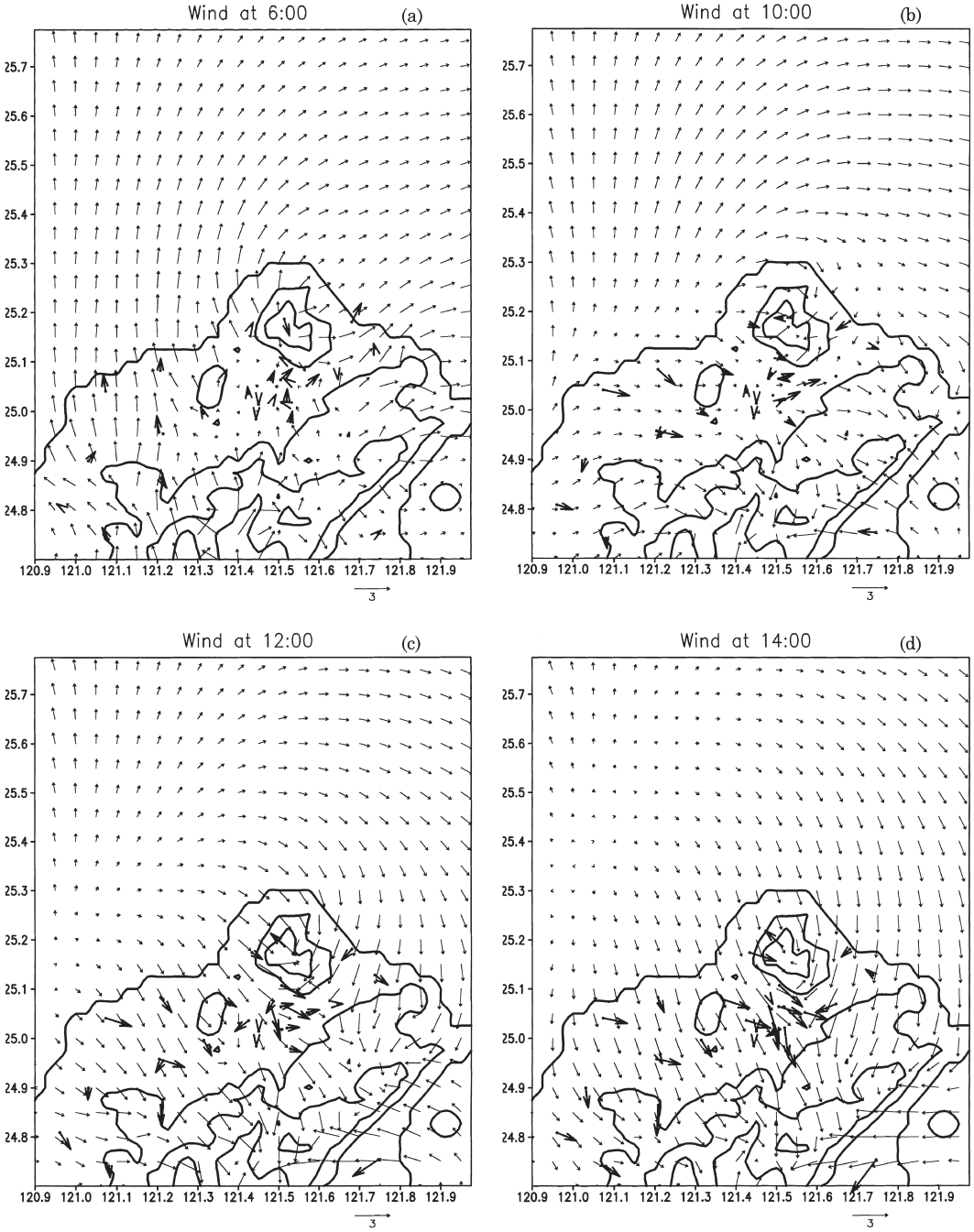
Wind at 6:00
(a)
Wind at 10:00
(b)
Wind at 12:00
(c)
Wind at 14:00
(d)
25.7
25.6
25.5
25.4
25.3
25.2
25.1
25.0
24.9
24.8
120.9 121.0 121.1 121.2 121.3 121.4 121.5 121.6 121.7 121.8 121.9
3

Fig. 5.

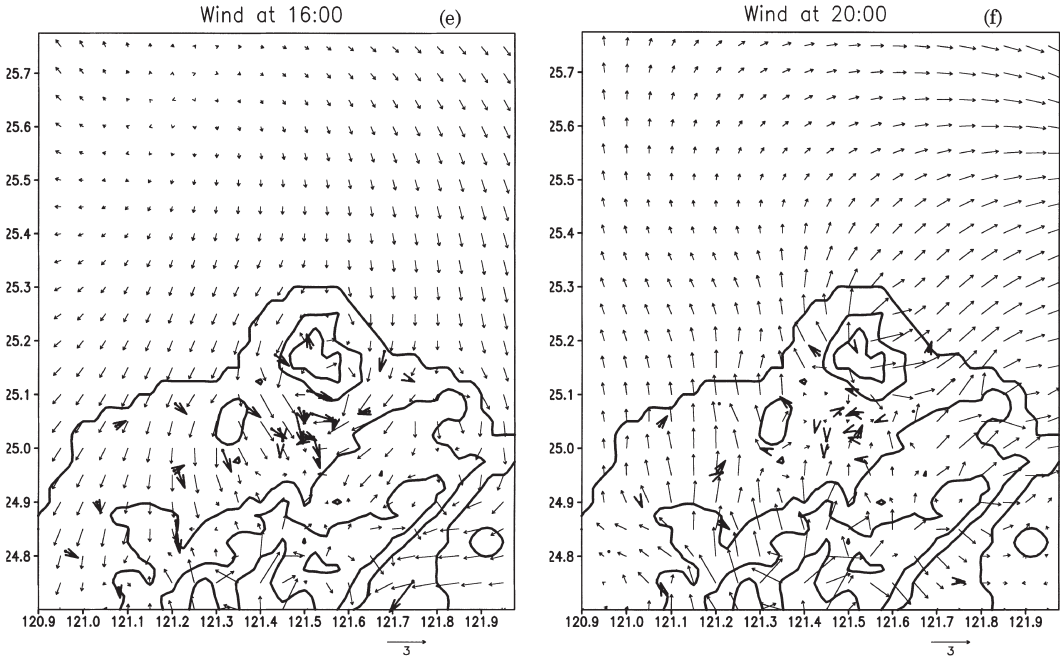

Fig. 5. Computed wind fields at the 10 m level above surface for (a) 06:00, (b) 10:00, (c) 12:00, (d) 14:00, (e) 16:00, and (f) 20:00 LT on 16 November 1998. Thick arrows represent observed surface winds (m/s). Thick solid lines are terrain contours representing 0, 200, 500 and 1000 m MSL.

the early morning (Fig. 5a), the surface wind field is dominated by a land breeze in the northern coastal areas and over the surrounding sea. The numerical results show good agreement with observed winds. The mountain valley winds also exist in the Xueshan Mountains. At 08:00 LT, the wind speed is very low throughout the whole Taipei basin. It is the time when 2 wind regimes change. After a significant temperature difference between the land and sea has developed, sea breezes are driven in the coastal areas. The shift in wind direction from south to west is clearly seen in the southwest part of the model domain, which agrees well with the observations (Fig. 5b). The intensity and extent of the sea breeze increase with time, and by 14:00 LT, the northwest and northeast winds into the Taipei basin are more than 2 ms^{-1} through the two valleys (Figs. 5c, d).

On the other hand, the wind caused by the steep mountains in the southern part of the model domain is also influenced significantly. At 18:00 LT, the wind from south in the Xueshan Mountains has a peak. By that time, the sea breeze has been weakened due to the decreasing temperature difference between the land and sea. However, the sea breeze still remains in the coastal areas. The wind speed is very low in the southern part of the Taipei basin where the 2 wind regimes meet (Fig. 5e). The sea breeze disappears at 20:00 LT and the wind from the mountains develops and covers the land, winds are still very weak in the basin (Fig. 5f). The numerical results agree well with observations, both in wind direction and in wind speed. Thus, flow patterns during the high-ozone episode are controlled mainly by the local terrain, and resulted from the imbalance between the forcing from the large-scale pressure system and that of differential heating/cooling of the basin, valleys, mountains and sea.

Fig. 6 presents comparisons of averaged observed and predicted wind speeds at the different stations in the model domain. Group A (locations 1–3) represents the coastal area in the northeast part of the domain. Group B (locations 4–16) is situated in the Taipei basin, and group C (locations 18–24) represents the southwestern part of the domain. Group D (location 64) is located at 500 m high on the mountain. The peak patterns

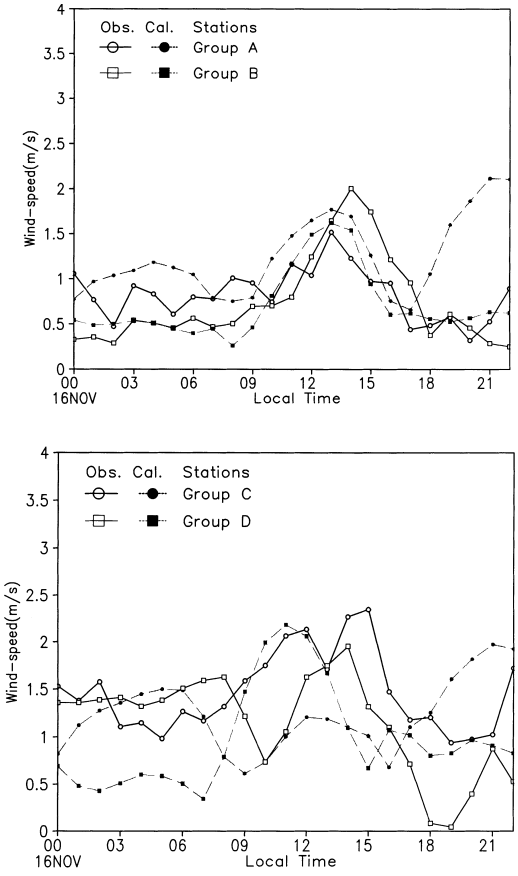

Fig. 6. Comparison of observed and predicted wind speeds averaged over some locations in the northern Taiwan for 16 November 1998. Station groups are listed in Fig. 1. The dashed and solid lines are the predicted and observed values, respectively.

of predicted wind speed agree with observations quite well, except for locations 18–19, where predicted high wind speeds lag from the observed ones. Comparisons with observed and predicted wind vectors indicate that the MMPMS is capable of simulating the general features of the winds in the northern Taiwan area.

4.2. *Air pollution situation*

Predicted horizontal distributions of surface NO_X and O_3 concentrations are shown in Figs. 7, 8. Observed values are also plotted in the figures. Fig. 7a shows the distribution of the predicted NO_X at 08:00 LT. The concentrations are over 90 ppb in the Taipei basin, similar to the observed values, although some values over 150 ppb are not predicted well. In general, the predicted concentrations follow reasonably well the observed concentrations. The ozone levels at that time are quite low, less than 30 ppb, showing good agreement with observation (Fig. 8a). The transport of pollutants from the Taipei basin is directed to the north–northeast. Ozone has been transported to the sea in the morning, because the coastal areas are still controlled by the land breeze (Fig. 5a). At 12:00 LT, the NO_X concentrations have decreased much more and reach low levels less than 60 ppb in the whole model domain. When pollutants return back toward the Taipei basin by the northwesterly and northeasterly sea-breezes through the 2 valleys (Fig. 5c), the photochemical process is very active, which causes a very high ozone concentration (Fig. 8b). NO_X concentrations show little increase at 16:00 LT (Fig. 7c), but ozone levels have decreased much more, from more than 100 ppb to less than 60 ppb in the Taipei basin. The observations also show the same trend (Fig. 8c). At 20:00 LT, the sea breeze disappears and the wind speeds in the basin are very low; thus, the primary pollutants such as NO_X are crammed into a shallow basin (Fig. 7d). The very low concentrations of ozone in the city appear because of depletion by the concentrated NO_X (Fig. 8d).

A scatterplot gives a clear visual picture of correlation between observed and predicted values, and it is important to supplement the statistical measures of agreement which will be discussed later. Thus, scatter diagrams for hourly O_3, and NO_X concentrations are shown in Fig. 9 in which all the observed values at monitoring stations are plotted, and thus some data points are in the same grid points in the model simulation. A reasonable correlation between observed and predicted values is obtained in these figures, although some points lay far from a straight line. The numerical results reveal an underestimation for all pollutants. The correlation coefficients of O_3, NO_X, and SO_2 are 0.83, 0.72 and 0.68, respectively. A better predictive performance for O_3 would be obtained if ozone peak values were not underestimated at noon-time. One reason may be the delay of the appearance time of the sea-breeze in simulation. Underestimation in the top-left corner of the scatter diagram of NO_X probably

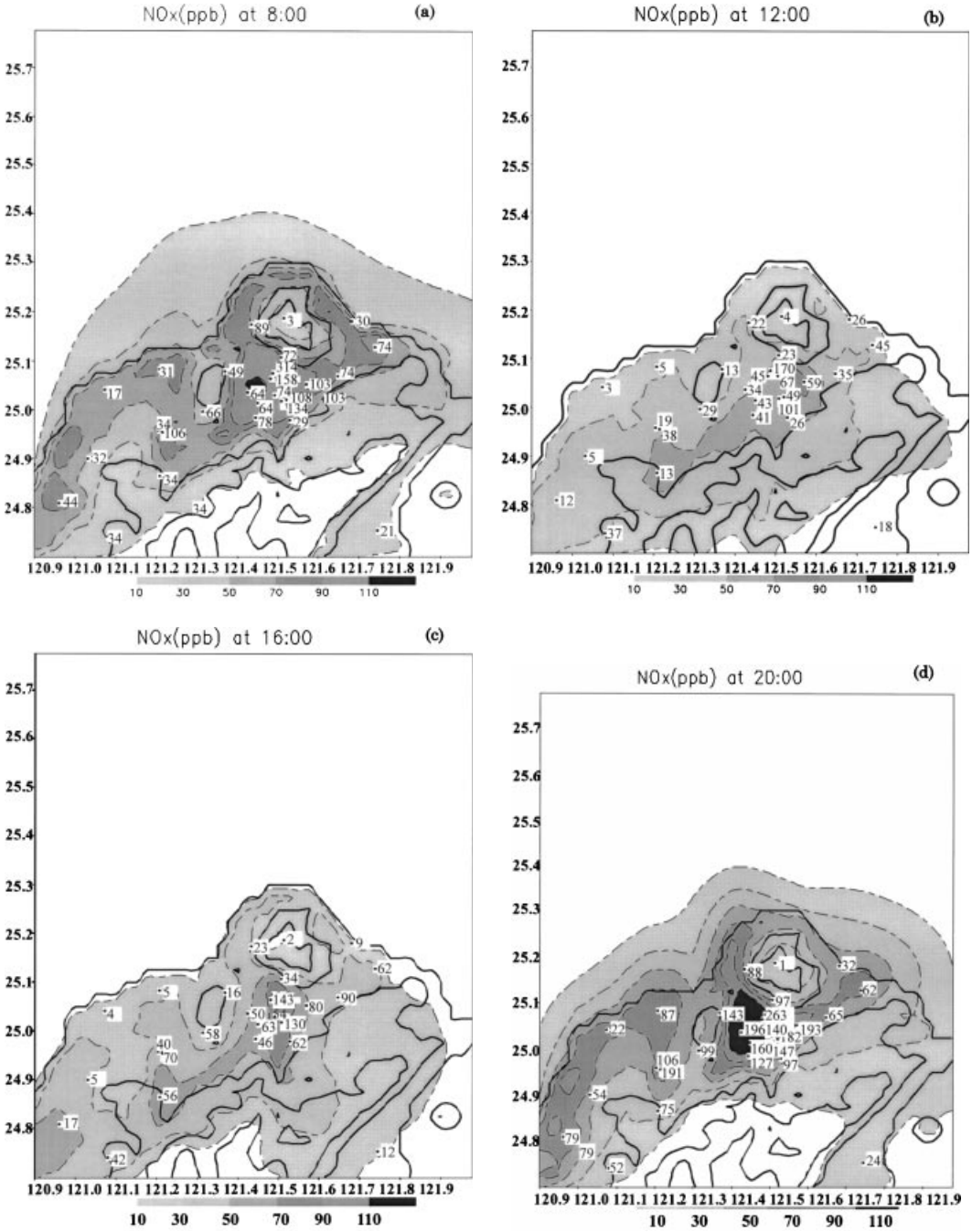

Fig. 7. Computed surface NO_X (ppb) concentration for (a) 08:00, (b) 12:00, (c) 16:00, and (d) 20:00 LT on 16 November 1998. Thick solid lines are terrain contours representing 0, 200, 500 and 1000m MSL. Numbers on the background are values of observed concentration.

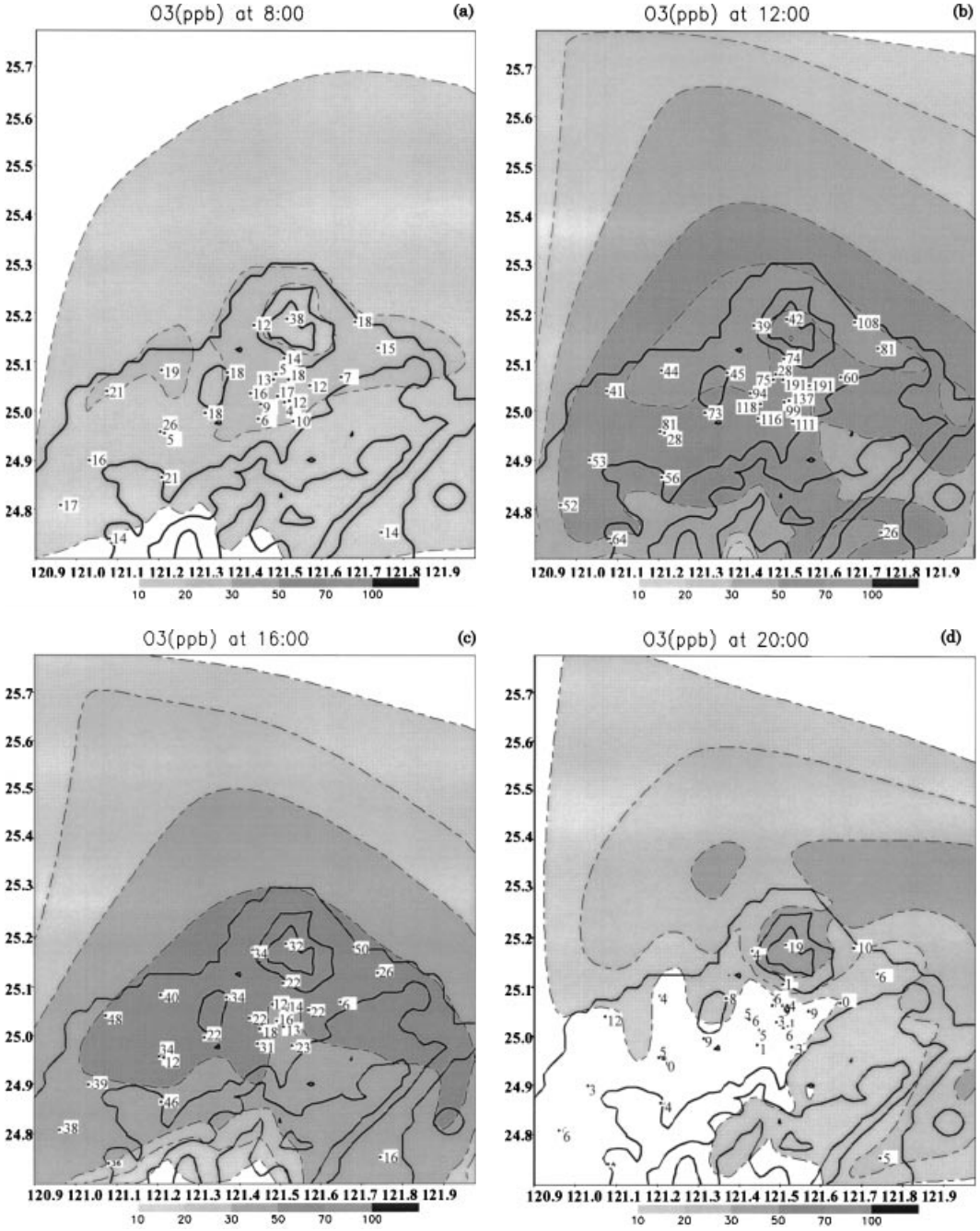

Fig. 8. Same as Fig. 7 except for O_3.

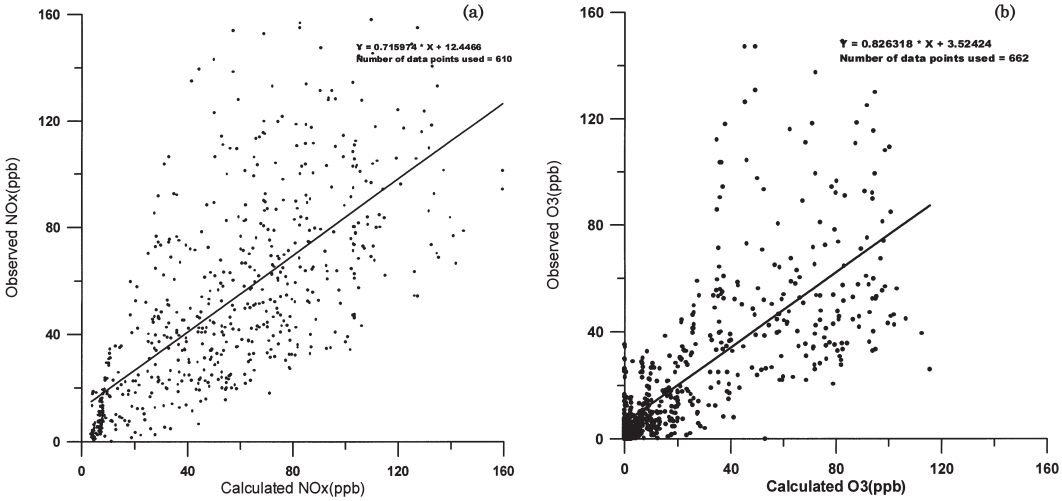

Fig. 9. Scatterplot diagram for the calculated and observed surface concentrations for (a) NO_X, and (b) O_3 on 16 November 1998 at 29 locations in the northern Taiwan.

corresponds to the direct influence of emissions on a local scale.

Comparisons of diurnal variations for observed and predicted concentrations of NO_X, and O_3 at different locations in the model domain are presented in Figs. 10, 11. There are double peaks in the observed NO_X levels for most locations except for the locations 64, where the anthropogentic emissions are lower than the urban areas (Fig. 10). The predicted values show the same double peaks, in spite of slightly lower peak values, except for group B. The appearance times of the peaks also agree well with the observations. Between the 2 peaks, there is a trough at noon-time. That is considered to be due to the active photochemical transformation into nitrate, the thick mixing layer and the reduced emission from traffic. In the Taipei basin (group B), the agreement between the observation and prediction looks much better than for other sites. At most of the stations, the predicted phases of the diurnal ozone variation are in accord with observations (Fig. 11). In the Taipei basin, the peak of observed ozone levels appeared at noon-time, which is similar to the predicted peak level but with a time lag of 2 h. The agreement in the southwest coastal area is much better with nearly the same peak value (Fig.11). The predicted tendency of the diurnal ozone variation agrees well with observations for the mountain sites. The similar performance is seen for SO_2 which has double peaks in the morning and in the evening, respectively (not shown).

4.3. Error checks

A series of statistical measures of the agreements or disagreements between the predicted and observed values are used to quantify the model performance. These include the mean error (ME), the mean normalized bias (MNB), the mean bias (MB), the mean absolute normalized gross error (MANGE), the paired peak estimation accuracy and the temporally paired peak estimation. Assume that there are n measurement stations, each performing m measurements during the evaluation period. Let $P_{i,j}$ and $O_{i,j}$ be the predicted and observed concentrations of a species for the station i during the j interval, respectively. According to Seinfeld and Pandis (1997), the above parameters are defined by

$$\mathrm{ME} = \frac{1}{nm}\sum_{i=1}^{n}\sum_{j=1}^{m}|P_{i,j} - O_{i,j}|, \tag{4}$$

$$\mathrm{MNB} = \frac{1}{nm}\sum_{i=1}^{n}\sum_{j=1}^{m}\frac{P_{i,j} - O_{i,j}}{O_{i,j}}, \tag{5}$$

$$\mathrm{MB} = \frac{1}{nm}\sum_{i=1}^{n}\sum_{j=1}^{m}P_{i,j} - O_{i,j}, \tag{6}$$

$$\mathrm{MANGE} = \frac{1}{nm}\sum_{i=1}^{n}\sum_{j=1}^{m}\frac{|P_{i,j} - O_{i,j}|}{O_{i,j}}. \tag{7}$$

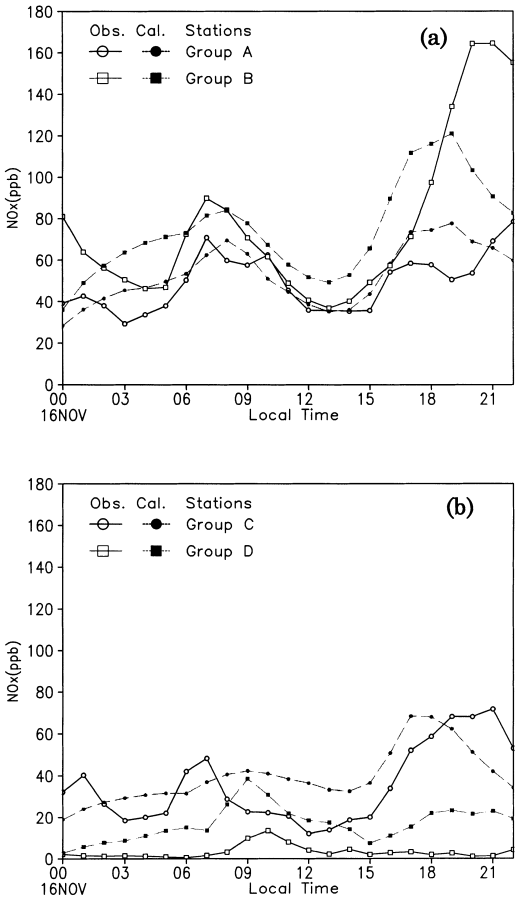

Fig. 10. Same as Fig. 6 except for NO_X (ppb).

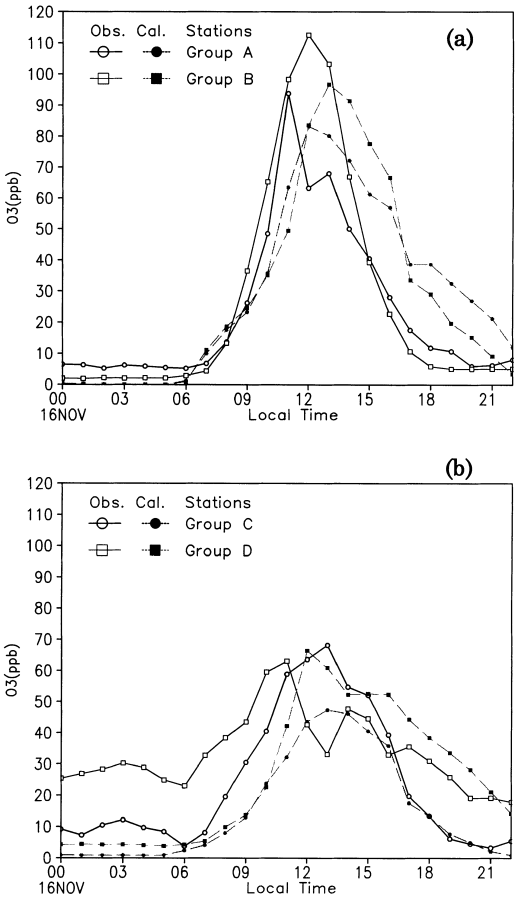

Fig. 11. Same as Fig. 6 except for O_3 (ppb).

The gross errors and biases of wind, O_3, NO_X, SO_2 and PM10 both for the 24-h period simulation and for daytime have been calculated with the above methods and are listed in Table 2. It shows that the normalized gross errors in O_3, NO_X, SO_2 and PM10 concentrations are between 34.4% and 36.8% for the 24-h simulation, while they vary from 24.3% to 36.5% for daytime. The predicted normalized biases for ozone are -6% and -11% for the 24-h simulation and for daytime, respectively. The predicted levels of all pollutants are lower than the observations, with the mean normalized biases less than -10%. It is probably due to a relatively large model resolution of 3 km adopted in the present model, which could not capture the intense local emissions in the urban areas. Although the mean absolute normalized gross error MANGE of ozone for daytime keeps the same level as that for 24-h simulation, those for other pollutants exibits some improvements in the daytime simulation, especially for SO_2 and PM10.

Statistics for surface wind speed and wind direction are also listed in Table 2. The normalized gross error in wind speeds, determined over the 24-h period simulation, is 38.9%, and the bias is low, i.e., the mean normalized bias is -12.1%. In spite of the very low mean wind speed of 1.2 ms^{-1}, the predictions for the wind speed are quite good. Furthermore, the normalized errors and biases are much lower at daytime when the sea breeze is dominant in the region. However, the model predicted the wind direction with larger errors and biases.

Table 2. *The mean absolute normalized gross error (MANGE), the mean normalized bias (MNB), the mean error (ME), the mean bias (MB), and the average values for predicted (CAL) and observed (OBS) wind and pollutants for both the entire 24-h simulation and for noon-time*

Parameter	No.	MANGE (%)	MNB (%)	MB	ME	CAL	OBS
			24-h simulation from 0:00 LT, 16 November 1998				
SO_2	665	34.4	−1.5	−1.7	3.7	8.0	9.7
O_3	663	35.9	−6.0	−6.7	13.8	29.7	36.3
NO_X	666	34.7	−5.2	−14.0	27.5	59.8	73.7
PM10	662	36.8	−8.1	−6.0	29.0	77.1	83.0
wind-speed	608	38.9	−12.1	−0.2	0.4	0.9	1.2
wind-direction	434	37.8	−24.6	−72.3	87.7	153.5	225.7
			Statistics only for noon-time (from 12:00 to 15:00 LT)				
SO_2	115	30.9	−6.9	−1.4	2.5	6.4	7.8
O_3	117	36.5	−11.2	−20.6	32.4	59.0	79.6
NO_X	113	33.3	4.3	−3.9	16.0	38.6	42.5
PM10	117	24.3	−4.5	−8.6	23.0	89.7	98.4
wind-speed	95	33.2	−7.2	−0.3	0.6	1.4	1.7
wind-direction	74	52.7	−45.2	−128.1	132.2	126.2	254.3

N.B.: The second column in the table is the number of observations for which data are available during the period of statistics; 3rd to 6th columns are the mean absolute normalized gross error, the mean normalized bias, the mean error, the mean bias, the mean predicted values and observed values. The units of MB, ME, CAL and OBS are as follows: ppb for SO_2, O_3, NO_X, $\mu g/m^3$ for PM10, m/s for wind speed and degrees for wind direction.

4.4. Effects of emissions

In order to study the sensitivity of NO_X and NMHC emissions in northern Taiwan, 2 simulations are performed in which NO_X and NMHC emissions are halved, respectively. Fig. 12 shows the response of ozone formation to the 50% reduction of NMHC emission. The ozone concentration decreases at all sites during the simulation period. The case for NO_X emission halved is presented in Fig. 13. This shows that ozone levels do not always decrease for the reduction of NO_X emission. There is a kind of tendency: the ozone level increases when NO_X levels are high, while it decreases for low NO_X levels. The ozone level is predicted to be reduced more effectively by the NMHC emission control, especially when NO_X levels are more than 100 ppb. At that time, NO_X emission control results in an increase in ozone concentration. In contrast, NO_X emission control is more effective for reduction of ozone level when NO_X concentrations are lower than 20 ppb.

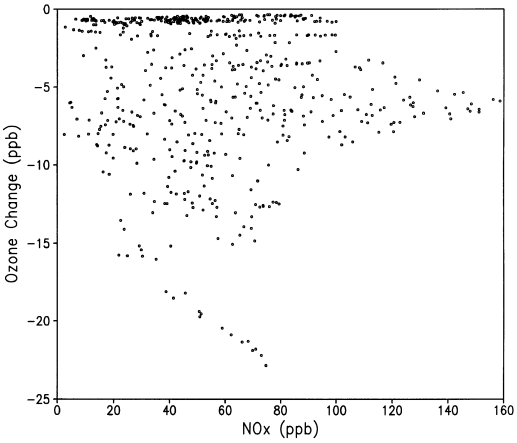

Fig. 12. Response of ozone concentration to 50% cut of NMHC emission for 27 stations at different NO_X concentration levels in northern Taiwan. Each point represents hourly-averaged concentration on 16 November 1998. The vertical axis is the ozone concentration in the emission control case subtracted from the base case concentration.

5. Conclusions

An air pollution prediction system (APOPS) has been developed for air quality studies in regional and local scales. The APOPS treats meteorology, tracer transport and diffusion, and gas-phase chemistry processes interactively. In the APOPS, a meteorological model (MMPMS)

solves the 3-dimensional, non-hydrostatic equations of fluid dynamics and thermodynamics over complex terrain, and incorporates the key physical processes that control the boundary layer behavior. A tracer transport model (GATAM) computes the advection, diffusion, emission, deposition, and chemical process in which the comprehensive gas-phase chemistry mechanisms are considered.

The flow patterns typical of the mountain-valley winds and sea/land breezes under stagnant synoptic weather conditions in northern Taiwan area are well replicated in APOPS. The general characteristics of surface distributions of ozone, SO_2, NO_X and aerosols have been simulated and assessed. The overall agreement between predictions and observations for this case shows that the current model system can be utilized to study the air pollution in the urban scale due to photochemical oxidants and other pollutants in the complex terrain regions. More model simulations for other observations should be applied for a generalization of the system.

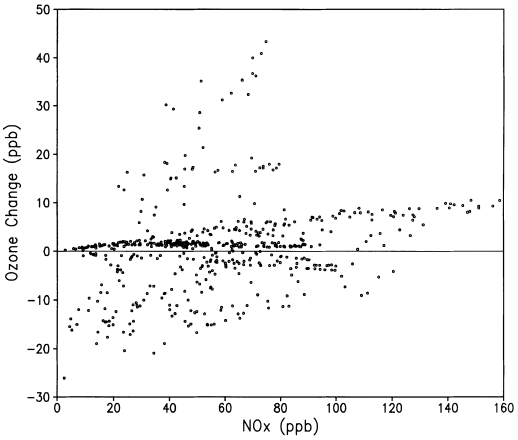

Fig. 13. Response of ozone concentration to 50% cut of NO_X emission for 27 stations at different NO_X concentration level in northern Taiwan. Each point represents an hourly averaged concentration on 16 November 1998. The vertical axis is the ozone concentration in the emission control case subtracted from the base case concentration.

6. Acknowledgement

Support for this research was partly provided by the Chinese Academy of Science (Key Project (A) KZ951-A1-403-01). Datasets of TAQMN are provided by the Taiwan EPA project (EPA-88-FA32-03-2114). The authors would like to thank the anonymous referee for valuable critical reviews, which helped to improve this manuscript.

REFERENCES

Buckley, R. L. and Kurzeja, R. J. 1997a. An observational and numerical study of the nocturnal sea breeze, Part I: Structure and circulation. *J. Appl. Meteorol.* **36**, 1577–1598.

Buckley, R. L. and Kurzeja, R. J. 1997b. An observational and numerical study of the nocturnal sea breeze, Part II: Chemical transport. *J. Appl. Meteorol.* **36**, 1599–1619.

Carmichael, G. R., Peters, L. K. and Kitada, T. 1986. A second-generation model for regional-scale transport/chemistry/deposition. *Atmos. Environment* **20**, 173–188.

Carter, W. P. L., Lurmann, F. W., Atkinson, R. and Lloyd, A. C. 1986. *Development and testing of a surrogate species chemical reaction mechanism.* EPA/600/3-86-031. US Environmental Protection Agency, Research Triangle Park, NC.

Chang, J. S., Broast, R. A., Isaksen, I. S. A., Madronich, S., Middleton, P., Stockwell, W. R. and Walcek, C. J. 1987. A three-dimensional Eulerian acid deposition model. Physical concepts and model formulation. *J. Geophy. Res.* **92**, 14681–14700.

Chang, Y.-S., Carmichael, G. R., Kurita, H. and Ueda, H. 1989. The transport and formation of photochemical oxidants in central Japan. *Atmos. Environment* **23**, 363–393.

Dodge, M. C. 1989. A comparison of three photochemical oxidant mechanisms. *J. Geophy. Res.* **94**, 5121–5136.

Gery, M. W., Whitten, G. Z., Killus, J. P. and Dodge, M. C. 1989. A photochemical kinetics mechanism for urban and regional scale computer modeling. *J. Geophys. Res.* **94**, 12,925–12,956.

He, D. and Huang, M. Y. 1992. A photochemical model for regional air quality simulation. *J. Environ. Sci.* **12**, 192–198.

Hurley, P. J. and Manins, P. C. 1995. Meteorological modeling on high-ozone days in Perth, Western Australia. *J. Appl. Meteorol.* **34**, 1643–1652.

Kitada, T. and Kitagawa, E. 1990. Numerical analysis of the role of sea breeze fronts on air quality in coastal and inland polluted areas. *Atmos. Envion.* **24A**, 1545–1559.

Liu, C. M., Liu S. C. and Shen, S. H. 1990. A study of

Taipei ozone problem. *Atmos. Environment* **24**, 1461–1472.

Liu, K. Y., Wang, Z., Tseng, H. Y. and Hsiao, L. F. 1999. *Study of the distribution and reduction process of ozone and other pollutants in Taiwan.* EPA-88-FA32-03-2114, Taiwan Environmental Protection Agency, Taipei, Taiwan.

Lu, R. and Turco, R. P. 1997. An integrated air pollution modeling system for urban and regional scales: 1. Structure and performance. *J. Geophys. Res.* **102D**, 6063–6079.

Moussiopoulos, N. 1995. The EUMAC zooming-model, a tool for local scale regional air quality study. *Metero. Atmos. Phys.* **57**, 115–133.

Scheffe, R. D. and Morris, R. E. 1993. A review of the development and application of the urban airshed model. *Atmos. Environment* **27B**, 23–39.

Seinfeld, J. H. and Pandis, S. N. 1997. *Atmospheric chemistry and physics: from air pollution to climate change.* John Wiley & Sons Inc., p. 1239.

Sha, W., Kawamura, T. and Ueda, H. 1991. A numerical study on sea/land breezes as a gravity current: Kelvin–Helmholtz billows and inland pentration of the sea-breeze front. *J. Atmos. Sci.* **48**, 1649–1665.

Sha, W., Kawamura, T. and Ueda, H. 1993. A numerical study of nocturnal sea breezes: Prefrontal gravity waves in the compensating flow and inland penetration of the sea-breeze cutoff vortex. *J. Atmos. Sci.* **50**, 1076–1088.

Sha, W., Grace, W. and Physick, W. 1996. A numerical experiment on the Adelaide gully wind of South Australia. *Aust. Met. Mag.* **45**, 19–40.

Svensson, G. 1995a. A numerical model for chemical and meteorological processes in the atmospheric boundary layer. Part I: A model description and a one-dimensional parameter study. *J. Appl. Meteorol.* **35**, 939–954.

Svensson, G. 1995b. A numerical model for chemical and meteorological processes in the atmospheric boundary layer. Part II: A case study of the air quality situation in Athens, Greece. *J. Appl. Meteorol.* **35**, 955–973.

Wakamatsu, S., Ohara, T. and Uno, I. 1998. Springtime photochemical air pollution in Osaka: model analysis. *J. Appl. Meteorol.* **37**, 1107–1116.

Wang, Z., Huang, M., He, D., Xu, H. and Zhou, L. 1996. Sulfur distribution and transport studies in East Asia using Eulerian model. *Advances in Atmospheric Sciences* **13**, 399–409.

Walcek, C. J. and Aleksic, N. M. 1998. A simple but accurate mass conservative peak-preserving, mixing ratio bounded advection algorithm with Fortran code. *Atmos. Environment* **32**, 3863–3880.

Yamartino, R. J., Scire, S., Carmichael, G. R. and Chang, Y. S. 1992. The CALGRID mesoscale photochemical grid model-I. Model formulation. *Atmos. Environment* **26A**, 1493–1512.